Chemosphere 355 (2024) 141765

Contents lists available at ScienceDirect

Chemosphere

journal homepage: www.elsevier.com/locate/chemosphere

Impact of airborne iron oxide nanoparticles on *Tillandsia usneoides* as a model plant to assess pollution in heavy traffic areas

Sara Falsini [a], Ilaria Colzi [a], Marco Dainelli [a], Elia Parigi [b], Maria Cristina Salvatici [c], Alessio Papini [a], Delphine Talbot [d], Ali Abou-Hassan [d,e], Cristina Gonnelli [a,*], Sandra Ristori [b]

[a] Department of Biology, University of Florence, Via Micheli 1-3, 50121 Florence, Italy
[b] Department of Chemistry and CSGI, Università degli Studi di Firenze, Via della Lastruccia 3-13, 50019 Sesto Fiorentino, Italy
[c] Institute of Chemistry of Organometallic Compounds (ICCOM)-Electron Microscopy Centre (Ce.M.E.), National Research Council (CNR), via Madonna del Piano n. 10, 50019 Sesto Fiorentino, Firenze, Italy
[d] Sorbonne Université, CNRS, PHysico-chimie des Electrolytes et Nanosystèmes InterfaciauX, PHENIX, F-75005 Paris, France
[e] Institut Universitaire de France (IUF), 75231 Paris Cedex 05, France

HIGHLIGHTS

- Toxicity of airborne magnetite nanoparticles was tested on *Tillandsia usneoides*.
- Biometry and ionome, but not photosynthesis, were altered by the treatment.
- Small nanoparticles were localised on the trichome wings.
- Small nanoparticles were more toxic than large ones for *T. usneoides*.

GRAPHICAL ABSTRACT

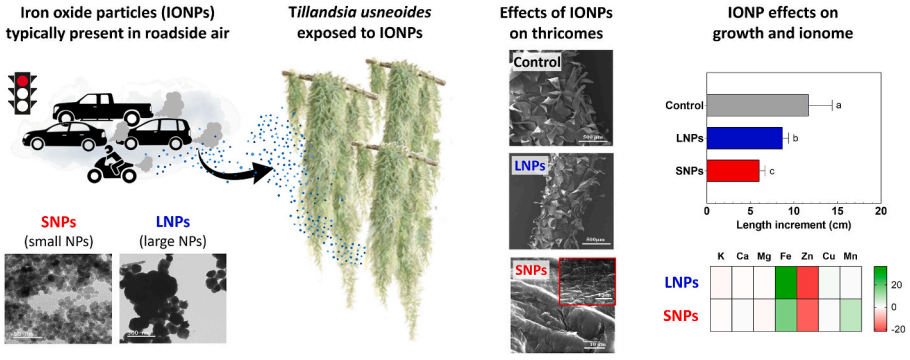

ARTICLE INFO

Handling Editor: Lena Q. Ma

Keywords:
Environmental biomonitoring
Atmosphere pollution
Magnetite particles
Epiphytic plants
IONPs

ABSTRACT

Due to the increasing evidence of widespread sub-micron pollutants in the atmosphere, the impact of airborne nanoparticles is a subject of great relevance. In particular, the smallest particles are considered the most active and dangerous, having a higher surface/volume ratio. Here we tested the effect of iron oxide (Fe_3O_4) nanoparticles (IONPs) with different mean diameter and size distribution on the model plant *Tillandsia usneoides*.

Strands were placed in home-built closed boxes and exposed to levels of airborne IONPs reported for the roadside air, i.e. in the order of 10^7 - 10^8 items m^{-2}. Plant growth and other morpho-physiological parameters were monitored for two weeks, showing that exposure to IONPs significantly reduced the length increment of the treated strands with respect to controls. A dose-dependence of this impairing effect was found only for particles with mean size of a few tens of nanometers. These were also proved to be the most toxic at the highest concentration tested. The IONP-induced hamper in growth was correlated with altered concentration of macro- and micronutrients in the plant, while no significant variation in photosynthetic activity was detected in treated

Abbreviations: IONPs, iron oxide nanoparticles; LNPs, large nanoparticles; SNPs, small nanoparticles; LC, low concentration; HC, high concentration.

* Corresponding authorphone number: +39 055 2757384.
E-mail address: cristina.gonnelli@unifi.it (C. Gonnelli).

https://doi.org/10.1016/j.chemosphere.2024.141765
Received 29 January 2024; Received in revised form 19 March 2024; Accepted 20 March 2024
Available online 24 March 2024

samples. Microscopy investigation showed that IONPs could adhere to the plant surface and were preferentially located on the trichome wings.

Our results report, for the first time, evidence of the negative effects of airborne IONP pollution on plant health, thus raising concerns about related environmental risks.

Future research should be devoted to other plant species and pollutants to assess the impact of airborne pollution on plants and devise suitable attenuation practices.

1. Introduction

Iron oxide particles (IONPs) in the form of magnetite (Fe_3O_4) are found as finely dispersed pollutants in the atmosphere (Li et al., 2021), especially in regions where anthropogenic activities are intensive (Zhang et al., 2020). These particles are mostly originated in dense traffic areas and industrial districts, such as cement factories, power industries and exhausted vehicle deposits. Air pollution caused by IONPs has been reported as a major problem either in open spaces or in the lab (Abdul-Razzaq and Gautam, 2001; Verma et al., 2016), thus attracting the attention of public institutions and the scientific community. As other polluting particles (i.e., nano- and microplastics) (Kumar et al., 2021), IONPs can be taken up and internalized by living organisms (Oberdörster et al., 2004). In humans, they are accumulated in various tissues, such as the brain and the pleura, or are absorbed by the serum (Singh and Sanjeeb, 2014). In particular, it has been shown that, when the diameter of these particles is less than approximately 200 nm (Wohlfart et al., 2012; Maher et al., 2016), they can cause severe neurodegenerative diseases since they are able to cross the blood-brain barrier through the olfactory neural pathway (Hamdy et al., 2022a). Reports indicate the impact of airborne IONP pollution as negative and harmful for humans (Zhu et al., 2019) and animals (Kaloyianni et al., 2020), though plant-based green synthesis of IONPs with reduced toxicity has been proposed for their medical applications (Hamdy et al., 2022b, 2022c). In any case, their effect on plants has not been investigated yet, albeit these organisms have a universally acknowledged role as primary producers and climate regulators (Fankhauser et al., 2022; Matzka and Maher, 1999). Actually, leaves are among the principal targets for airborne pollution agents, since their large (smooth or faceted) surfaces can absorb many contaminants, either in the form of molecules or particulates (Omasa et al., 2002), including magnetic particles derived from vehicle emission (Prajapati et al., 2006). As for other environmental matrices, such as soil and water, information about the relationship between IONPs and plants is found with rather variable outcomes, according to administration modality and particle concentration. Until now, studies on soil have been mainly focused on plant nutrition, possibly overlooking the problem of toxicity by IONP high levels, even though these particles can be found at considerable concentrations in some backgrounds, such as roadside terrains (Liu et al., 2022). On the other hand, researchers dealing with Fe deficiency and low availability in plants (Vose, 1982) have proposed the administration of magnetite nanoparticles as a strategy for promoting plant growth in nano-enabled agriculture (Singh et al., 2021). According to some studies, this strategy would also contribute to decrease environmental pollution caused by classical fertilizers (Dola et al., 2022; Ahmed et al., 2023). Concerning water environments, IONP pollution is reported to have a negative impact on plant growth and development (Jafarirad et al., 2019; Giorgetti et al., 2011; Li et al., 2015). For example, the excess of IONPs in hydroponics has been shown to reduce plant biomass production, through induction of oxidative stress and decrease of photosynthetic pigment contents (Wang et al., 2011; Li et al., 2020). Conversely, low concentrations of Fe-containing particles in hydroponics and their administration as foliar spray are reported to induce positive effects on plants (Tombuloglu et al., 2019; Iannone et al., 2016) included the reduction of heavy metal toxicity (Emamverdian et al., 2023). In any case, IONPs used in controlled conditions have been proposed for wastewater treatment (Yadav et al., 2020; Rajendran et al., 2023).

Due to the assessed presence of IONPs in the atmosphere and their predictable increasing levels in the future, these particles are to be considered a possible environmental threat. Investigating whether airborne IONP contamination can affect plant growth and development becomes of fundamental importance for the scientific community in view of actions to preserve the overall functioning of the biosphere. Here, the problem of airborne magnetite nanoparticle pollution on plants was addressed by using the model species *Tillandsia usneoides* (L.) L. The neotropical genus *Tillandsia* offers the possibility to estimate contaminants in the atmosphere, as these plants take up water and nutrients directly from the air due to the lack of a root apparatus (Mosti et al., 2008). *Tillandsia* species present leaf trichomes with an external wing of dead cells and a stem able to absorb water and nutrients (Papini et al., 2010), thus making this plant a valuable tool for biomonitoring atmospheric pollutants (Brighigna et al., 2002). Moreover, *Tillandsia usneoides* is present in a wide range of environments, from Florida to Argentina (Sun et al., 2021), and has already been used as a sensor of airborne pollution (Schreck et al., 2020; Falsini et al., 2022).

Two types of magnetite nanoparticles with different mean size and polydispersity were chosen as models of IONP pollution and were tested on *T. usneoides* cultivated in controlled conditions. This choice stems from the evidence that smaller particles have a higher impact due to their extended surface on equal conditions of chemical composition and mass. On the other hand, particles with wide size distribution represent a realistic model to study pollution by airborne finely dispersed materials which can be generated by different fractioning processes, thus resulting in inhomogeneous size and shape. The aims of this work were: i) assessing if *T. usneoides* is sensible to realistic concentrations of airborne IONPs by evaluating changes in growth, chlorophyll fluorescence and element concentration, ii) investigating possible IONP adhesion to the plant surface by SEM microscopy, iii) evaluating whether IONP dimension can differently affect their toxicity to our plant system.

This report is the first to study the consequences of airborne magnetite pollution on plants and opens new questions on the already serious issue that the excess of nanoparticles can impact living organisms, claiming awareness for its control and reduction.

2. Materials and methods

2.1. Magnetic nanoparticles, plant material and experimental conditions

Magnetite bare nanoparticles were purchased in powder by Merck and Co., Inc (CAS N° 1317-61-9). Interestingly, these particles have a size distribution that closely resemble the one occurring at a short distance, i.e. 20 m, from a roadside soil (Prajapati et al., 2006) and were considered as large nanoparticles (LNPs). Small magnetite nanoparticles (SNPs) were synthesized by the well-known Massart process by alkaline co-precipitation of Fe^{3+} and Fe^{2+} precursors (Martens et al., 2019; Bertuit et al., 2022). Briefly, 0.9 mol of $FeCl_2 \bullet 4H_2O$ and 1.6 mol of $FeCl_3 \bullet 6H_2O$ were co-precipitated by 7 mol of alkaline ammonium solution. After magnetic decantation, the obtained magnetic particles were isolated and washed several times with nitric acid, acetone, and diethyl ether to remove excess precursors and by-products. At the end of this process, the SNPs were re-suspended in water. SNPs and LNPs were diluted in Milli-Q water at a final iron concentration of about 0.1 g mL^{-1} and a drop of the solutions was deposited on carbon-coated grids and

imaged by transmission electron microscopy using a JEOL-1011 at 100 kV. The size distribution histograms of the two different sizes of nanoparticles were analysed from the TEM images using ImageJ software (https://imagej.nih.gov/). The histograms were fitted by a LogNormal function.

To administer IONPs to plants, a home-built setup was used as described by Falsini et al. (2022). In each box, nine *T. usneoides* strands with a length of approximately 30 cm were hung to the lid by the hooks. The air circulation was guaranteed by two fans located at the opposite side of the box, directed toward the bottom to create a turbulent motion. These fans were programmed to switch on during the night for a total time of 2h when CAM species like *T. usneoides* open the stomata (Martin and Siedow, 1981). Two beakers filled with demineralized water were placed in the box to maintain humidity; the exchange of air with the external environment was promoted by two circular openings present on the opposite side of the box. Finally, all the boxes were placed in a growth chamber with the following conditions: 24/16 °C day/night, light intensity 300 μmol m^{-2} s^{-1}, 16-h (day) photoperiod and relative humidity 60–65%.

Tillandsia usneoides plants were purchased at a local nursery (Giulio Celandroni Orchidee, San Giuliano Terme, Pisa) and maintained in the growth chamber with the conditions indicated above. Single strand length was measured and samples of homogeneous size and with a similar number of ramifications, not more than 5, were chosen for the trial. The length measurements were performed by analysing the images of the plants with ImageJ, adding all the ramifications length. Thus, the cumulative length of the plants was calculated. The stem diameter was measured as well and resulted constant.

Tillandsia usneoides strands were exposed to IONPs having size and concentrations typically present in polluted air environments (Magiera et al., 2011), specifically, in the roadside air i.e. in the order of 4×10^7 items m^{-2} and 4×10^8 items m^{-2} (Maher et al., 2016). The calculation of the IONPs amount to be allocated in each prototype chamber was based on the volume of the particles, considering that particles showed a spherical shape of known mean diameter, whose value was extracted as the mean of the corresponding size distribution. The highest polluted atmosphere was replicated in a box of 18 dm^3 by administering a total of 3.1×10^{-3} μg and 1.04×10^{-4} μg for LNPs and SNPs, respectively while the lowest polluted air was obtained by resuspending 3.1×10^{-4} μg and 1.04×10^{-5} μg for LNPs and SNPs respectively. The acronyms of the different samples are listed in Table 1.

To obtain these amounts of particles a series of dilutions was operated starting from a stock solution of 2 g mL^{-1}. Droplets of 31 μL of both types of NPs were placed on a plastic disk under fans before switching on. The fans, being directed downward, were able to induce a circular movement of the IONPs into the box after drying the droplets. During exposure, each *T. usneoides* strand was hydrated with 5 mL of sprayed tap water three times a week. In this same period, increment in plant growth was calculated by subtracting length values at the beginning of the treatment to values at 3, 7, 11 and 14 days of treatment. At each step in which the chambers were opened to make measurements, IONPs were newly administered to maintain the initial amount of particles.

Table 1
List of acronyms referring to the different samples used in *T. usneoides* treatments where H and L mean high and low, respectively.

Sample Name	Sample acronym
Control	CNT
LNPs 4×10^7 items/m^3 o $1. \times 10^{-4}$ μg	LC-LNPs
LNPs 4 10^8 items/m^3 o 3×10^{-3} μg	HC-LNPs
SNPs 4×10^7 items/m^3 o 1×10^{-4} μg	LC-SNPs
SNPs 4 10^8 items/m^3 o 3×10^{-3} μg	HC-SNPs

LC = Low Concentration; LNPs = Large Nanoparticles; HC= High Concentration; SNPs = Small Nanoparticles.

2.2. Fluorescence parameters

Chlorophyll fluorescence was measured using a portable fluorimeter (Plant Efficiency Analyzer – Handy PEA, Hansatech Instruments Ltd) on 15-min dark-adapted leaf samples flashed for 1 s with a saturated (1800 μmol m^{-2} s^{-1}) LED red light pulse (650 nm). The potential quantum efficiency of photosystem II Fv/Fm (Fv if the variable fluorescence and indicates the difference between the maximal Fm and the minimal F0 fluorescence) and the general indicator of photosystem I and II efficiency Pindex (Performance index) were recorded.

2.3. Element determination

After the treatment, strands were dried at 70 °C for two days for the measurement of the concentration of micro- and macro-elements. 100 mg of oven-dried plant material was digested using 10 mL of 69% HNO_3 in a microwave digestion system (Mars 6, CEM) with a maximum temperature of 200 °C for 10 min (Bettarini et al., 2019). The amount of K, Ca, Mg, Fe, Zn, Cu and Mn was determined by atomic absorption spectroscopy (PinAAcle 500, PerkinElmer) with certified reference materials (grade BCR, Fluka Analytical, Sigma-Aldrich, method reliability and accuracy with values < 10% and <5% RDS respectively).

2.4. Scanning electron microscopy (SEM)

Scanning electron microscopy (SEM) measurements were performed at the CEME-Centro di Microscopie Elettroniche "Laura Bonzi", CNR Research Area (Florence, Italy). A Gaia 3 (Tescan s.r.o, Brno, Czech Republic) focused ion beam-scanning electron microscope electron beam used for SEM imaging had a voltage of 10 kV and was operating in a high vacuum and with a secondary electron detector. Gaia 3 was equipped with an EDS-X-ray microanalysis system (EDAX, AMETEK, USA) TEAM EDS Basic Software Suite TEAM™.

Samples were deposited on a stub, dried in a vacuum and then coated with an ultrathin coating of silver to enhance the contrast thanks to the presence of an electrically conducting material. Microanalysis was performed to identify the presence of nanoparticles on leaf surfaces.

To assess the dimension of trichomes from IONP-exposed samples, for each SEM image three trichomes with the whole surface horizontally visible were selected. Length and width of the wing and diameter of the shield were measured, and values were pooled together to obtain a mean value for each image. Three SEM images were analysed for each plant to obtain a mean value to be considered as the final value of the replicate.

2.5. Statistics

The experiment comprised five groups of plants (control plants and plants treated with the two kinds of IONPs at low and high concentrations) and for each group there were nine biological replicates. When measurements were performed over time (plant length increment and chlorophyll fluorescence), the same plant sample was investigated at different times. Linear regression was used to analyse experimental data of plant growth (GraphPad Prism 7, GraphPad Software, San Diego, CA), where the dependent variable was plant length increment while the independent one was sampling time. The angular coefficient (slope) of the linear regression was considered as a descriptor of the plant growth rate (Falsini et al., 2022). The significance of differences ($p < 0.05$) among means at the same experimental times (and among the slope values) was checked by one-way ANOVA using GraphPad Prism 7 (GraphPad Software, San Diego, CA). A HSD-Tukey test was run for post-hoc comparisons. The Shapiro-Wilk test was used to check data normality. Plant length increment, Fv/Fm and Pindex data were analysed by fitting linear mixed-effects models (LMMs) in a repeated measurement ANOVA design, considering plant identity as a random effect factor to account for the temporal correlation of observations. Time was used as an ordinal variable. The physiological effects of the treatment

were investigated using plant length increment, Fv/Fm and Pindex values as response variables and the treatments with IONPs as explanatory variables in a full factorial design. ANOVA type III table, with Satterthwaite's method, was used to prove the significance of the fixed effects and associated interaction factors. The analysis was run with the software R and LMM computations were performed using the lmer function of the lme4 package version 1.1–12 for model fitting.

3. Results

3.1. IONPs characterization

TEM images of magnetite SNPs and LNPs and their size distribution fitted by a Log-normal law are reported in Fig. 1A and B, respectively. As shown from these histograms, the two sets of nanoparticles were both monomodal and therefore suited to report on the effects induced by pollutants within a defined size range. Moreover, the average diameters of the two distributions were representative of the most commonly found for inorganic nanoparticles of metal oxides, with the largest particles having wider polydispersity. TEM images showed that the magnetite SNPs were predominantly spherical in shape with average diameter $d_0 = 13$ nm and $\sigma = 0.24$. By comparison, the LNPs showed marked variations in their morphology. In this case, the best-fit curve gave a (mean) diameter distribution centered at $d_0 = 230$ nm and $\sigma = 0.38$.

3.2. Impact of MNPs on plant growth and photosynthetic parameters

Concerning growth, control plants showed an increment in length over time (Fig. S1), whereas exposure to IONPs caused a significant reduction of plant length at any of the investigated exposure times ($265.9 < F < 703.7$ and $P < 0.0001$). At the end of the treatment, the increment in length was significantly different also among particle-exposed specimens, with HC-SNPs plants showing the lowest values (Fig. 2A). The increment variation depended significantly on the IONPs used (treatment*time significant with $P < 0.001$, Table S1). As the regression analysis gave significant results for the correlation between increment in length and sampling time (Fig. 2B–S1), the angular coefficient (slope) of this regression line was used to estimate the growth rate itself as in Falsini et al. (2022). This coefficient indicated significant differences among treatments ($F = 216.5$, $P < 0.0001$). All the values obtained for exposed specimens were lower than for control plants, having similar values in the case of LC-LNP, HC-LNP and LC-SNP samples and the lowest one for HC-SNP samples.

Concerning chlorophyll fluorescence, the Fv/Fm and Pindex values in control and treated samples over the whole exposure time are reported in Figs. S2 and S3, respectively. One-way ANOVA did not show any significant change among the different treatments at any time, despite an incipient lowering of Fv/Fm values occurring in treated plants toward the end of the experiment. The interaction treatment*time was not significant either (Tables S2 and S2).

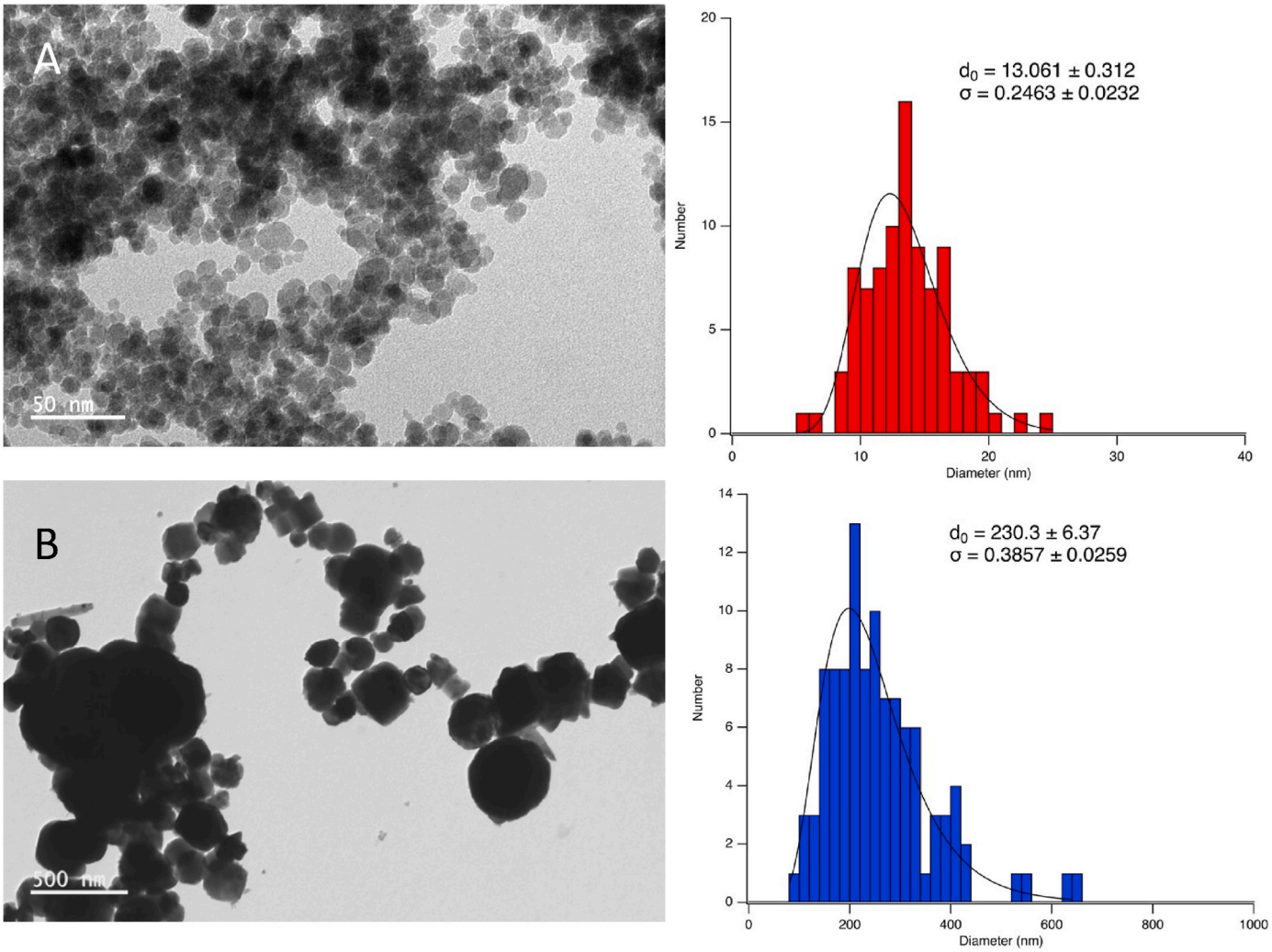

Fig. 1. Representative TEM micrographs of IONPs and their relative size distribution fitted by a Log-normal law with d_0 and σ as parameters. (A) SNPs (B) LNPs.

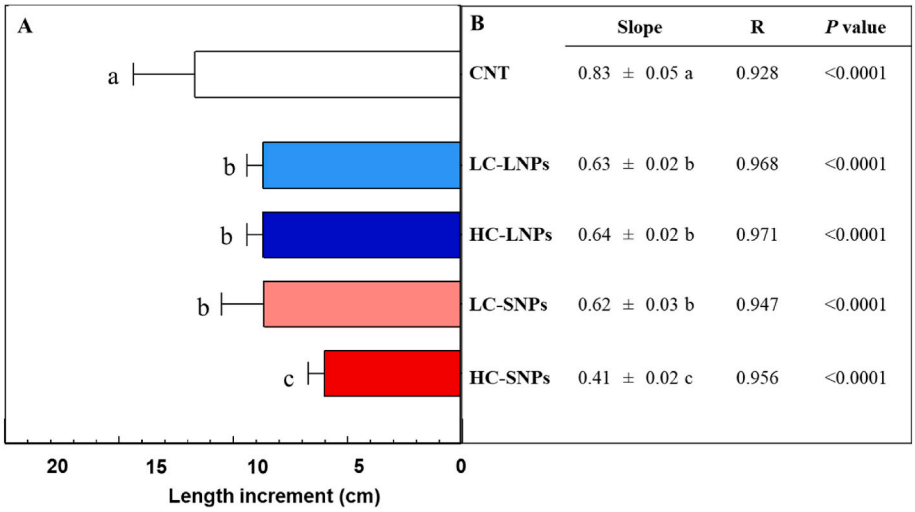

Fig. 2. A) Final increment in length (cm) of *Tillandsia usneoides* strands exposed to four types of NPs for 14 days. The increment was calculated by subtracting length values at the beginning of the treatment to the values measured at the end of the treatment. Letters close to the histograms indicate significant differences among treatments, according toTukey's test (at least $p < 0.01$). The reported values are means of 9 replicates + standard deviation. B) Growth rate of *T. usneoides* strands exposed to four types of NPs for 14 days calculated as the slope of the linear regression between plant length increment and sampling time.

3.3. IONP effect on the concentration of macro- and microelements

Table 2 reports the effects of the type and dose of IONPs on the concentration of some macro- and micronutrients in plant specimens. Differences among the treatments were highlighted by one-way ANOVA for half of the elements tested ($0.5925 < F < 8.122$ and $p < 0.0001$). In particular, IONPs exposure did not significantly alter the plant levels of Potassium (K), Calcium (Ca) and Copper (Cu), whereas all the treatments induced a significant decrease in Zinc (Zn) and Magnesium (Mg) accumulation, with the exception of the lowest MNP concentration. A general increase was found in the case of Iron (Fe), significantly for HC-LNPs exposure, and in the case of Manganese (Mn), significantly for HC-SNPs exposure.

The amplitude of the treatment-induced changes in element concentration depended both on the IONP-administered and the element under consideration, as evidenced by the heatmaps (Fig. 3), where the red colour indicates samples with decreased element concentration with respect to the control and the green colour indicates samples with increased element concentration with respect to the corresponding control. In general, the variations were similar for both kinds of IONPs, with no evident dose-dependency and with remarkable intensity only for Fe and Zn.

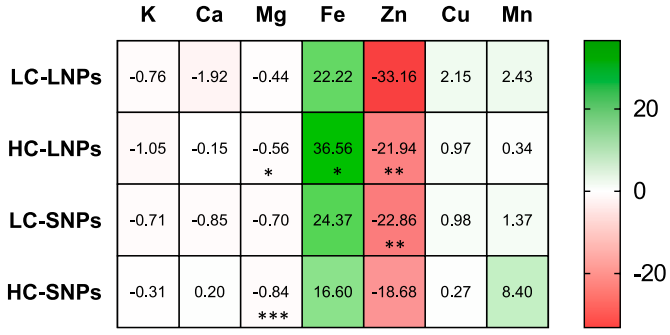

Fig. 3. Heatmaps of ionome variation in strands *Tillandsia usneoides* plants after 14 days of growth in the presence of LC-LNPs, HC-LNPs, LC-SNPs and HC-SNPs. Colour scale indicates increased (green), unchanged (white) or decreased (red) element concentration in respect to the corresponding control plants. Asterisks indicate significant differences between treated samples and control samples referred to Table 1 (* = $p < 0.05$, ** = $p < 0.01$, *** = $p < 0.001$). (For interpretation of the references to colour in this figure legend, the reader is referred to the Web version of this article.)

3.4. Microscopy on Tillandsia usneoides

The investigation performed by Scanning Electron Microscopy (SEM) showed that the trichome wings covered completely the epidermis of *T. usneoides* stem (Fig. 4A, B and C) in all the samples. Trichomes displayed the shape typical for *Tillandsia*, with a central shield and a wing forming a rhombus, or better a kite, in which an axis is longer than the other. The main axis was indicated here as "length" and the minor axis as "width". The most distal part of the wing was recurved outwards (Fig. 4A, B and C). Table 3 reports the average dimensions of the trichomes after exposure to the highest concentration of the IONPs. Control plants showed a trichome size of about 500 × 250 μm, with a mean shield diameter of around 85 μm. The treated samples showed a significant reduction of hair length ($F = 66.64$, $p < 0.0001$) for both kinds of IONPs, while the other parameters were not altered with respect to the control values. In control samples, no IONPs were detected (Fig. 4D), while many tiny dots smaller than 100 nm appeared on the trichome wings of plants treated with SNPs and could be interpreted as magnetite

Table 2
Element concentration (μg g^{-1} dry weight) in *Tillandsia usneoides* plants after 14 days of growth in the presence of pristine and aged MNPs. Values are mean of 9 replicates ± standard deviation. Asterisks indicate significant differences between treated samples and control samples (* = $p < 0.05$, ** = $p < 0.01$, *** = $p < 0.001$).

	K	Ca	Mg	Fe	Zn	Cu	Mn
CNT	11.27 ± 1.10 **a**	9.49 ± 1.97 **a**	1.76 ± 0.66 **a**	64.55 ± 16.07 **b**	93.75 ± 16.24 **a**	6.91 ± 1.54 **a**	31.67 ± 4.17 **b**
LC-LNPs	10.96 ± 2,01 **a**	9.28 ± 1.91 **a**	1.32 ± 0.37 **ab**	86.77 ± 25.33 **ab**	60.59 ± 6.51 **b**	9.07 ± 2.02 **a**	34.10 ± 4.16 **ab**
HC-LNPs	10.56 ± 1.14 **a**	9.13 ± 1.84 **a**	1.2 ± 0.27 **b**	101.11 ± 27.87 **a**	71.81 ± 11.70 **b**	7.89 ± 1.58 **a**	32.01 ± 4.20 **b**
LC-SNPs	10.5 ± 1.29 **a**	8.44 ± 1.28 **a**	1.06 ± 0.25 **b**	88.92 ± 28.45 **ab**	70.89 ± 13.77 **b**	7.89 ± 0.88 **a**	33.04 ± 5.53 **b**
HC-SNPs	10.22 ± 2.17 **a**	7.37 ± 2.2 **a**	0.92 ± 0.32 **b**	81.15 ± 21.83 **ab**	75.07 ± 13.30 **b**	7.18 ± 2.06 **a**	40.07 ± 6.50 **a**

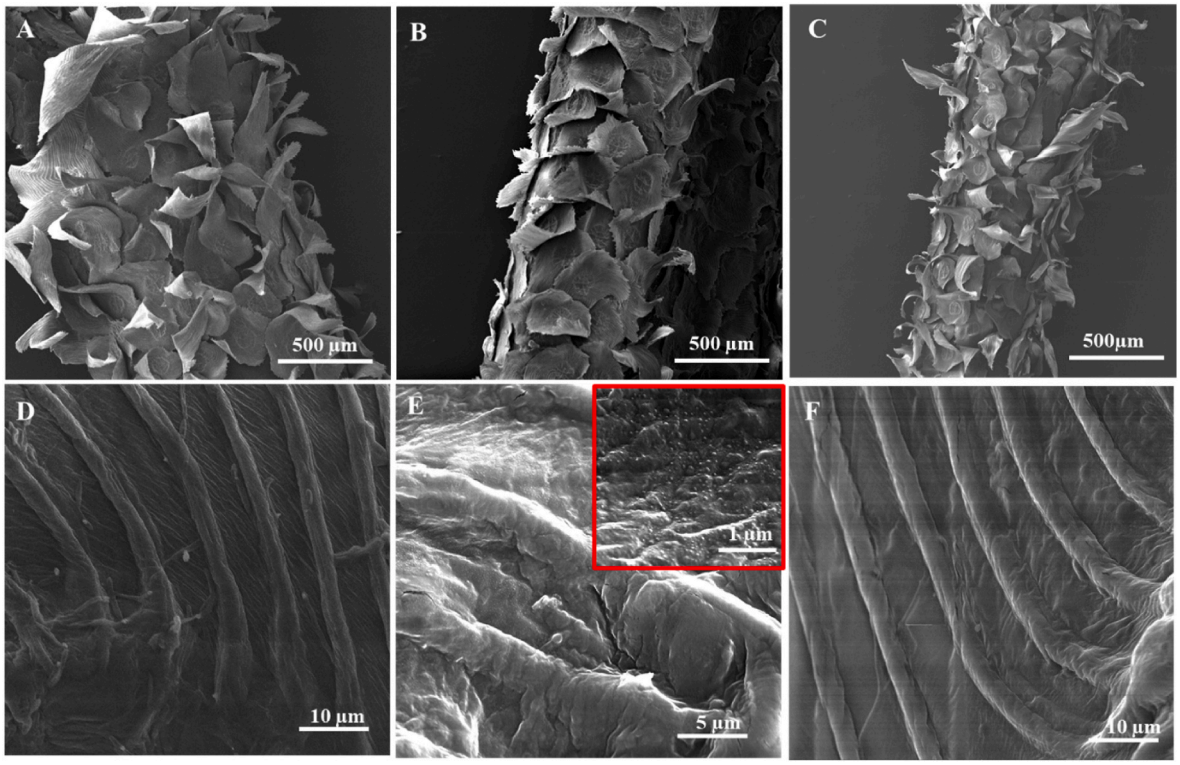

Fig. 4. SEM micrographs of *Tillandsia usneoides* morphology (new leaves) after 14 days of exposure to SNPs and LNPs. A) Control plants: trichomes covering completely the epidermis of the leaf. The trichomes are formed by a central shield (arrows) of 4 cells surrounded by 2 circles of cells and a large external wing (arrowheads) formed by dead cells. The wings overlap one with the other. B) plants exposed to SNPs. C) plants exposed to LNPs. D) Control plants: detail of the trichome wing. E) Detail of the trichome wing exposed to SNPs. Tiny dots smaller than 100 nm appear on the surface of the trichome. F) Detail of the trichome wing exposed to LNPs. Particles are not visible, but the surface of the wing appears corrugated.

Table 3
Dimension of *T. usneoides* trichomes in plants exposed for 14 days to small and large IONPs at the highest concentration. Values are mean of 9 replicates ± standard deviation. Lowercase letters indicate the significant differences among the treatments according to Tukey's test (at least $p < 0.05$).

	Hair length (µm)			Hair width (µm)			Shield diameter (µm)		
Control	523	±	36b	259	±	33 ab	85	±	11a
HC-SNPs	335	±	39a	267	±	36b	89	±	13a
HC-LNPs	362	±	37a	219	±	35a	81	±	7a

particles (Fig. 4E). Even though the surface of plants exposed to LNPs did not present any particle evidence, the exposure to these contaminants made the surface of the trichome wings appear peculiarly corrugated (Fig. 4F).

Microanalysis was performed on the trichome wing surface. As expected, while it did not record Fe in the control plants, both SNPs and LNPs treated samples showed a peak of iron (Fig. 5).

4. Discussion

All the experimental evidence reported in this work showed that airborne IONPs at environmentally relevant concentrations impaired *T. usneoides* growth, significantly already from the first exposure time for both types of particles tested and with a dose-depended effect only for the smaller ones. These also appeared more toxic than their larger counterparts, almost halving both plant length increment and growth rate when present at high concentrations. This marked toxicity shown by small magnetic particles and their concentration effect can be explained by a higher ability of small IONPs to enter the plant tissues and catalyse processes with negative influence on the plant health. The dimension of *Tillandsia* stomata around 50 µm (Martin and Peters, 1984) would allow the entry of both the nanoparticles here tested, but the thick layer of overlapping trichomes could represent a barrier. More probably, our ~13 nm IONPs were small enough to directly penetrate the plant body through possible discontinuities of the plant surface. Similar results, showing higher detrimental effects of small IONPs, supposedly due to their absorption, were also observed by Alkhatib et al. (2019) on tobacco plants exposed to particles in the same size range, even though administered to roots in hydroponics and therefore not directly comparable. Considering that in many contexts the main source of IONPs contamination comes directly from the atmosphere through road traffic, with a minor contribution from other anthropogenic activities (Magiera et al., 2011), our results point out the most critical matrix for studying magnetite nanoparticle administration to plants.

Regarding possible IONP toxicity mechanisms via limitations of photosynthesis, our data proved that at least for the concentrations and exposure times here tested, the reduction in plant growth could not be explained by a negative interference of airborne magnetite pollution with the photosynthetic process. Conversely, a negative effect of excessive amounts of iron oxide particles on several photosynthetic parameters has been reported when they are administered to roots in hydroponics (Alkhatib et al., 2019; Ursache-Oprisan et al., 2011), thus presenting again the difficulty of direct comparison among experiments with IONPs supplied through different routes. The IONPs impact on *T. usneoides* growth could be better explained if considering the particle-induced changes in the plant element concentration. Both types of IONPs caused the increase of Fe concentration and the decrease of Mg and, especially, Zn concentration. Even though the element levels did not fall outside the range commonly reported for plant shoots (Marschner, 1995; Kabata-Pendias and Pendias, 2001), the cumulative effect of the IONP-induced changes present in treated samples could have resulted in unbalanced development of *T. usneoides* plants. The observed Fe accumulation could derive both from the adhesion and/or

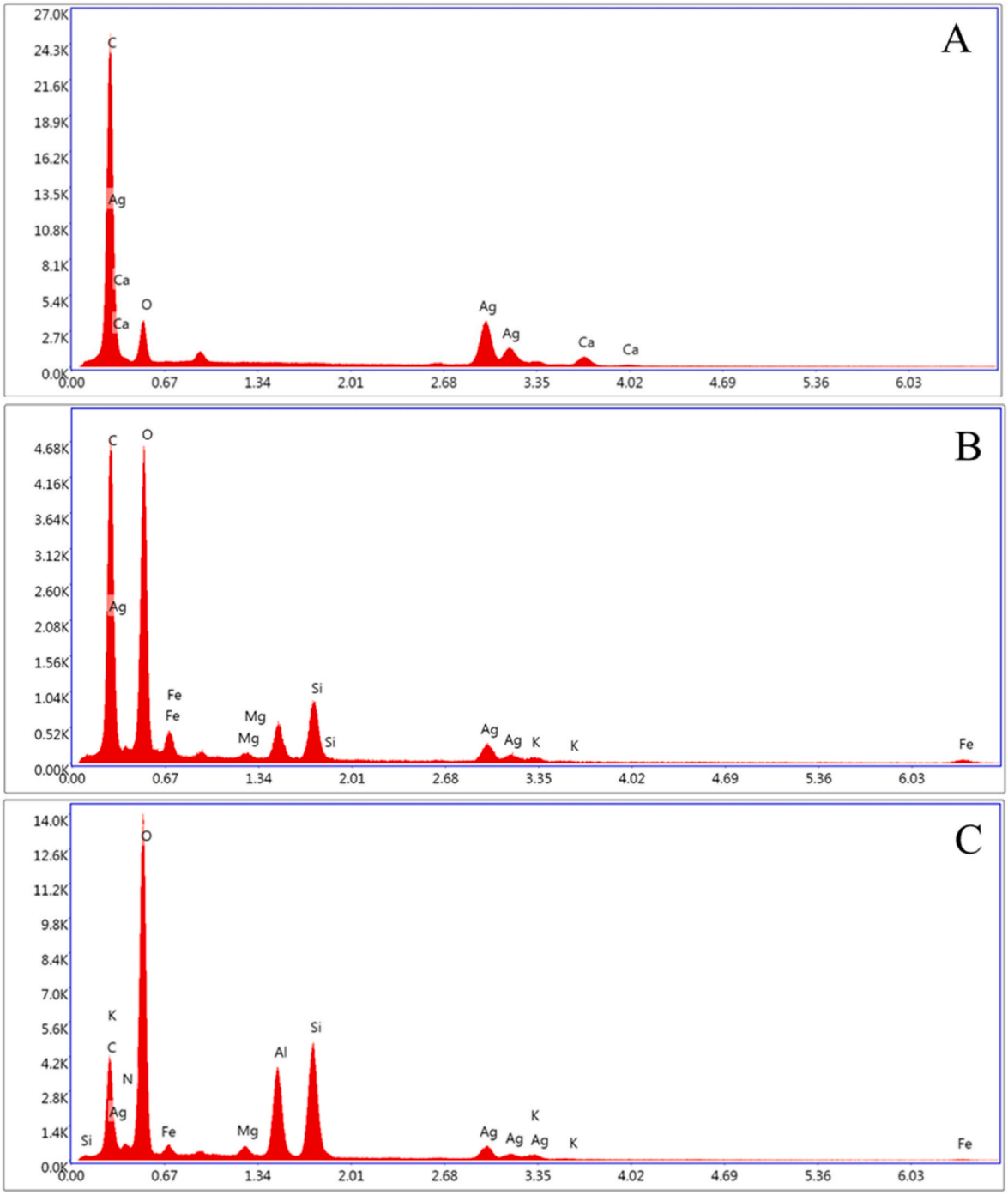

Fig. 5. Energy Dispersive X-ray spectroscopy microanalysis on control plants (a), plants exposed to SNPs (b) and plants exposed to LNPs (c).

entering of the IONPs in the plant or from the direct release of the metal from the IONPs, as proposed for trials in hydroponics and soil systems (Iannone et al., 2016; Yan et al., 2020; Deng et al., 2022). In our case, during the contact with the plant surface, the magnetic particles could leak Fe ions in the thin film of water that moves by capillarity among the overlapping trichomes of *Tillandsia* and is taken up by the plant together with the nutrients (Herppich et al., 2019). A consequence of this Fe-enrichment in the water entering the plant could be the observed decrease in Zn accumulation, since these two micronutrients share some common transporters (Colangelo and Guerinot, 2006) and therefore can compete for the same uptake systems. At the same time, Fe excess is known to negatively affect Mg availability to plants (Kirk et al.., 2022), thus causing the decrease recorded in the concentration of this other nutrient in IONP-treated *T. usneoides* strands. Following another study, the changes in the element profile could be explained considering that the IONPs generate a magnetic field which may alter the conductivity of the ion channels (Hughes et al., 2010). In fact, though the magnetic field generated by a nanoparticle is expected to be low, the effect of sharpness and fractal-like shape can play a role, as it is well established in the case of the electric field enhancement exploited by SERS (Boyacka and Le Ru, 2009).

SEM images provided information about the effect of IONPs on macro-morphological changes of the plant surface and their possible presence on the strands. Both kinds of magnetic particles were able to provoke a significant decrease in the length of *T. usneoides* trichomes. Since these structures are involved in water and ion uptake (Brighigna

et al., 2002; Mosti et al., 2008), the IONP-mediated reduction in their dimension could concur to explain the above-reported changes in the plant element profile, even though the mechanism by which the magnetic particles can affect the shape of the trichomes remains to be elucidated. In addition to the reduction in size, LNPs appeared to affect the distension of the wing itself, resulting in a corrugated surface that could have impaired the functioning of the trichomes. Regarding the presence of the particles on the strands, SEM images showed that apparently, only the smaller IONPs were able to adhere to the trichome surface, or at least to remain adhered thereafter the sample preparation, contrarily to the larger IONPs. This supposed stronger adherence of the SNPs to the trichomes might affect their functioning, contributing to determine their higher toxicity with respect to the LNPs. Furthermore, trichomes could represent a route for SNP entrance inside the mesophyll, thus concurring to increase their impact on *T. usneoides*. In any case, the preferential IONP localization was on the trichome wing and not on the central shield, as it was found for particles of plastic materials (Falsini et al., 2022). In addition, the microanalysis of the SEM images revealed the presence of Fe on the surface of the treated samples, even for LNP-treated plants where the detection of adhering particles was not possible. Probably, the enrichment of this element on the plant surface was due to the release of Fe from the particles themselves during their contact with the plant and, as regards SNPs, to the direct presence of the particles on the surface. In any case, even if the total amount of Fe did not exceed the toxicity limits, the enrichment of this element in the cells of the plant surface could have led to their impaired growth thus limiting the development of the whole strand. Actually, high concentrations of Fe are known to induce reductions in plant cell growth, with many toxicity mechanisms including ferroptosis (Distéfano et al., 2021).

5. Conclusions

Our results showed that airborne pollution at environmentally relevant IONP concentrations can impair the development of the model plant *Tillandsia usneoides*. Small IONPs were more toxic with respect to large ones; this effect can be traced back to their higher surface/volume ratio, which renders nanomaterials more reactive or prone to release metal ions, as well as to the enhanced ability of tiny objects to penetrate plant tissues. The observed hamper in plant growth was related to changes in the micro- and macro-elemental profile, though not in photosynthetic efficiency. IONPs were found to localize on the leaf trichomes and preferentially on their wings. While previous studies were mainly focused on the effects of IONPs administered by root exposure, thus taking into account contamination from water and soil, here we showed that also airborne magnetic particles can represent a threat to plant life.

This study draws attention to the possible harmful effects of airborne contaminants on plants, raising concerns about additional risks for the whole ecosystem. Further research should be undertaken not only to widen the investigated pollutants and species to complete the picture of this environmental issue, but also to devise strategies for its attenuation.

CRediT authorship contribution statement

Sara Falsini: Writing – review & editing, Methodology, Investigation, Formal analysis, Data curation, Conceptualization. **Ilaria Colzi:** Writing – review & editing, Supervision, Investigation, Formal analysis, Data curation, Conceptualization. **Marco Dainelli:** Writing – review & editing, Investigation, Formal analysis. **Elia Parigi:** Writing – review & editing, Methodology, Formal analysis. **Maria Cristina Salvatici:** Methodology, Investigation. **Alessio Papini:** Writing – review & editing, Resources, Data curation. **Delphine Talbot:** Writing – review & editing, Resources, Methodology, Formal analysis. **Ali Abou-Hassan:** Writing – review & editing, Resources, Methodology, Formal analysis. **Cristina Gonnelli:** Writing – review & editing, Writing – original draft, Supervision, Resources, Project administration, Methodology, Funding acquisition, Conceptualization. **Sandra Ristori:** Writing – review & editing, Supervision, Resources, Project administration, Methodology, Funding acquisition, Conceptualization.

Declaration of generative AI and AI-assisted technologies in the writing process

The authors declare no use of AI and AI-assisted technologies in the writing process.

Declaration of competing interest

The authors declare the following financial interests/personal relationships which may be considered as potential competing interests: Sara Falsini, Ilaria Colzi, Marco Dainelli reports financial support was provided by Ministry of Education and Merit. If there are other authors, they declare that they have no known competing financial interests or personal relationships that could have appeared to influence the work reported in this paper.

Data availability

Data will be made available on request.

Acknowledgements

This work was founded by the European Union - Next Generation EU. National Recovery and Resilience Plan (NRRP) - M4C2 Investment 1.3 - Research Programme PE_00000005 ″RETURN" - CUP B83C22004820002. Views and opinions expressed are however those of the author(s) only and do not necessarily reflect those of the European Union or the European Commission. Neither the European Union nor the European Commission can be held responsible for them. The publication was made with the contribution of the researcher Marco Dainelli with a research contract co-funded by the European Union - PON Research and Innovation 2014–2020 in accordance with Article 24, paragraph 3a), of Law No. 240 of December 30, 2010, as amended, and Ministerial Decree No. 1062 of August 10, 2021.

Thanks are due to Dr Silvia Schiff (Department of Biology, University of Florence) for fruitful discussions.

Appendix A. Supplementary data

Supplementary data to this article can be found online at https://doi.org/10.1016/j.chemosphere.2024.141765.

References

Abdul-Razzaq, W., Gautam, M., 2001. Discovery of magnetite in the exhausted material from a diesel engine. Appl. Phys. Lett. 78, 2018–2019.

Ahmed, M.A., Shafiei-Masouleh, S.S., Mohsin, R.M., et al., 2023. Foliar application of iron oxide nanoparticles promotes growth, mineral contents, and medicinal qualities of *Solidago virgaurea* L. J. Soil Sci. Plant Nutr. 23, 2610–2624. https://doi.org/10.1007/s42729-023-01218-2.

Alkhatib, R., Alkhatib, B., Abdo, N., AL-Eitan, L., Creamer, R., 2019. Physio-biochemical and ultrastructural impact of (Fe3O4) nanoparticles on tobacco. BMC Plant Biol. 19, 253. https://doi.org/10.1186/s12870-019-1864-1.

Bertuit, E., Benassai, E., Mériguet, G., Greneche, J.-M., Baptiste, B., Neveu, S., Wilhelm, C., Abou-Hassan, A., 2022. Structure–property–function relationships of iron oxide multicore nanoflowers in magnetic hyperthermia and photothermia. ACS Nano 16 (1), 271–284.

Bettarini, I., Colzi, I., Coppi, A., Falsini, S., Echevarria, G., Pazzagli, L., Selvi, F., Gonnelli, C., 2019. Unravelling soil and plant metal relationships in Albanian nickel hyperaccumulators in the genus *Odontarrhena* (syn. *Alyssum* sect. *Odontarrhena*, Brassicaceae). Plant Soil 440, 135–149.

Boyacka, R., Le Ru, E.C., 2009. Investigation of particle shape and size effects in SERS using T-matrix calculations. Phys. Chem. Chem. Phys. 11, 7398–7405. https://doi.org/10.1039/B905645A.

Brighigna, L., Papini, A., Mosti, S., Cornia, A., Bocchini, P., Galletti, G., 2002. The use of tropical Bromeliads (Tillandsia spp.) for monitoring atmospheric pollution in the town of Florence (Italy). Rev. De. Biol. Trop. 50 (2), 577–585.

Colangelo, E.P., Guerinot, M.L., 2006. Put the metal to the petal: metal uptake and transport throughout plants. Curr. Opin. Plant Biol. 9 (3), 322–330. https://doi.org/10.1016/j.pbi.2006.03.015.

Deng, C., Tang, Q., Yang, Z., et al., 2022. Effects of iron oxide nanoparticles on phenotype and metabolite changes in hemp clones (*Cannabis sativa* L.). Front. Environ. Sci. Eng. 16, 134. https://doi.org/10.1007/s11783-022-1569-9.

Distéfano, A.M., López, G.A., Setzes, N., Marchetti, F., Cainzos, M., Cascallares, M., Zabaleta, E., Pagnussat, G.C., 2021. Ferroptosis in plants: triggers, proposed mechanisms, and the role of iron in modulating cell death. J. Exp. Bot. 72 (6), 2125–2135. https://doi.org/10.1093/jxb/eraa425. PMID: 32918080.

Dola, D.B., Mannan, M.A., Sarker, U., Mamun, M.A.A., Islam, T., Ercisli, S., Saleem, M.H., Ali, B., Pop, O.L., Marc, R.A., 2022. Nano-iron oxide accelerates growth, yield, and quality of Glycine max seed in water deficits, 2022 Sep. 9 Front. Plant Sci. 13, 992535. https://doi.org/10.3389/fpls.2022.992535. PMID: 36160973; PMCID: PMC9500458.

Emamverdian, A., Ghorbani, A., Li, Y., Pehlivan, N., Barker, J., Ding, Y., Liu, G., Zargar, M., 2023. Responsible mechanisms for the restriction of heavy metal toxicity in plants via the Co-foliar spraying of nanoparticles. Agronomy 13, 1748. https://doi.org/10.3390/agronomy1307174.

Falsini, S., Colzi, I., Chelazzi, D., Dainelli, M., Schiff, S., Papini, A., Coppi, A., Gonnelli, C., Ristori, S., 2022. Plastic is in the air: impact of micro-nanoplastics from airborne pollution on Tillandsia usneoides (L.) L. (Bromeliaceae) as a possible green sensor. J. Hazard Mater. 437, 129314 https://doi.org/10.1016/j.jhazmat.2022.129314.

Fankhauser, S., Smith, S.M., Allen, M., Axelsson, K., Hale, T., Hepburn, C., Kendall, J.M., Khosla, R., Lezaun, J., Mitchell-Larson, E., Obersteiner, M., Rajamani, L., Rickaby, R., Seddon, N., Wetzer, T., 2022. The meaning of net zero and how to get it right. Nat. Clim. Change 12, 15–21.

Giorgetti, L., Castiglione, M.R., Bernabini, M., et al., 2011. Nanoparticles effects on growth and differentiation in cell culture of carrot. Daucus carota L.) Agrochimica 55, 45–53.

Hamdy, N.M., Shaker, F.H., Zhan, X., Basalious, E.B., 2022a. Tangled quest of post-COVID-19 infection-caused neuropathology and what 3P nano-bio-medicine can solve? EPMA J. 13, 261–284. https://doi.org/10.1007/s13167-022-00285-2.

Hamdy, N.M., Boseila, A.A., Ramadan, A., Basalious, E.B., 2022b. Iron oxide nanoparticles-plant insignia synthesis with favorable biomedical activities and less toxicity, in the "era of the-green": a systematic review. Pharmaceutics 14, 844. https://doi.org/10.3390/pharmaceutics14040844.

Hamdy, N.M., Eskander, G., Basalious, E.B., 2022c. Insights on the dynamic innovative tumor targeted-nanoparticles-based drug delivery systems activation techniques. Int. J. Nanomed. 17, 6131–6155.

Herppich, W.B., Martin, C.E., Totzkë, C., Manke, I., Kardjilov, N., 2019. External water transport is more important than vascular transport in the extreme atmospheric epiphyte Tillandsia usneoides (Spanish moss). Plant Cell Environ. 42 (5), 1645–1656. https://doi.org/10.1111/pce.13496.

Hughes, S., El-Haj, A.J., Dobson, J., Martinac, B., 2010. The influence of static magnetic fields on mechanosensitive ion channel activity in artificial liposomes. Eur. Biophys. J. 34 (5), 461–468.

Iannone, M.F., Groppa, M.D., de Sousa, M.E., Fernández van Raap, M.B., Benavides, M. P., 2016. Impact of magnetite iron oxide nanoparticles on wheat (*Triticum aestivum* L.) development: evaluation of oxidative damage. Environ. Exp. Bot. 131, 77–88.

Jafarirad, S., Ardehjani, P.H., Movafeghi, A., 2019. Are the green synthesized nanoparticles safe for environment? A case study of aquatic plant Azolla filiculoides as an indicator exposed to magnetite nanoparticles fabricated using microwave hydrothermal treatment and plant extract. Journal of Environmental Science and Health Part A-Toxic/Hazardous Substances & Environmental Engineering,CES 54 (6), 506–517.

Kabata-Pendias, A., Pendias, H., 2001. Trace Elements in Soils and Plant. CRC Press, Boca Raton.

Kaloyianni, M., Dimitriadi, A., Ovezik, M., Stamkopoulou, D., Feidantsis, K., Kastrinaki, G., Galliose, G., Tsiaoussis, I., Koumoundouros, G., Bobori, D., 2020. Magnetite nanoparticles effects on adverse responses of aquatic and terrestrial animal models. J. Hazard Mater. 383, 121204 https://doi.org/10.1016/j.jhazmat.2019.121204.

Kirk, G.J.D., Manwaring, H.R., Ueda, Y., Semwal, V.K., Wissuwa, M., 2022. Below-ground plant–soil interactions affecting adaptations of rice to iron toxicity. Plant Cell Environ. 45, 705–718. https://doi.org/10.1111/pce.14199.

Kumar, M., Chen, H., Sarsaiya, S., Qin, S., Liu, H., Awasthi, M.K., Kumar, S., Singh, L., Zhang, Z., Bolan, N.S., Pandey, A., Varjani, S., Taherzadeh, M.J., 2021. Current research trends on micro- and nano-plastics as an emerging threat to global environment: a review. J. Hazard Mater. 409, 124967 https://doi.org/10.1016/j.jhazmat.2020.124967.

Li, P.Y., Wang, A.D., et al., 2020. Insight into the interaction between Fe-based nanomaterials and maize (Zea mays) plants at metabolic level. Sci. Total Environ. 738.

Li, S., Zhang, B., Wu, D., Li, Z., Chu, S.-Q., Ding, X., Tang, X., Chen, J., Li, Q., 2021. Magnetic particles unintentionally emitted from anthropogenic sources: iron and steel plants. Environ. Sci. Technol. Lett. 8 (4), 295–300.

Li, X., Yang, Y., Gao, B., Zhang, M., 2015. Stimulation of peanut seedling development and growth by zero-valent iron nanoparticles at low concentrations. PLoS One 10 (4), e0122884. https://doi.org/10.1371/journal.pone.0122884.

Liu, L., Zhang, Q., Gui, J., Zhang, B., Yang, H., Lu, D., Chen, Z., Liu, Q., Li, Z., Jiang, G., 2022. Traffic-derived magnetite pollution in soils along a highway on the Tibetan Plateau. Environ. Sci.: Nano 9, 621–631.

Magiera, T., Jablonska, M., Strzyszcz, Z., Rachwal, M., 2011. Morphological and mineralogical forms of technogenic magnetic particles in industrial dusts. Atmos. Environ. 45 (25), 4281–4290.

Maher, B.A., Ahmed, I.A.M., Karloukovski, V., MacLaren, D.A., Foulds, P.G., Allsop, D., Mann, D.M.A., Torres-Jardon, R., Calderon-Garciduenas, L., 2016. Magnetite pollution nanoparticles in the human brain. Proc. Natl. Acad. Sci. USA 10797–10801.

Marschner, H., 1995. Mineral Nutrition of Higher Plants. Academic Press, London.

Martens, U., Böttcher, D., Talbot, D., Bornscheuer, U., Abou-Hassan, A., Delcea, M., 2019. Maghemite nanoparticles stabilize the protein corona formed with transferrin presenting different iron-saturation levels. Nanoscale 11, 16063.

Martin, C.E., Peters, E.A., 1984. Functional stomata of the atmospheric epiphyte *Tillandsia unseoides*. L. BOT. GAZ. 145 (4), 502–507.

Martin, C.E., Siedow, J.N., 1981. Crassulacean acid metabolism in the epiphyte *Tillandsia usneoides* L. (Spanish moss). Responses of CO_2 exchange to controlled environmental conditions. Plant Physiol 68, 335–339.

Matzka, J., Maher, B.A., 1999. Magnetic biomonitoring of roadside tree leaves: identification of spatial and temporal variations in vehicle-derived particulates. Atmos. Environ. 33 (28), 4565–4569. https://doi.org/10.1016/S1352-2310(99)00229-0.

Mosti, S., Papini, A., Brighigna, L., 2008. A new quantitative classification of ecological types in the bromeliad genus Tillandsia (Bromeliaceae) based on trichomes. Rev. De. Biol. Trop. 56 (1), 191–203.

Oberdörster, G., Sharp, Z., Atudorei, V., Elder, A., Gelein, R., Kreyling, W., Cox, C., 2004. Translocation of inhaled ultrafine particles to the brain. Inhalation Toxicol. 16 (6–7), 437–445.

Omasa, K., Tobe, K., Kondo, T., 2002. Absorption of organic and inorganic air pollutants by plants. In: Omasa, K., Saji, H., Youssefian, S., Kondo, N. (Eds.), Air Pollution and Plant Biotechnology. Springer, Tokyo. https://doi.org/10.1007/978-4-431-68388-9_8.

Papini, A., Tani, G., Di Falco, P., Brighigna, L., 2010. The ultrastructure of the development of Tillandsia (Bromeliaceae) trichome. Flora 205 (2), 94–100. https://doi.org/10.1016/j.flora.2009.02.001.

Prajapati, S.K., Pandey, S.K., Tripathi, B.D., 2006. Monitoring of vehicles derived particulates using magnetic properties of leaves. Environ. Monit. Assess. 120, 169–175. https://doi.org/10.1007/s10661-005-9055-y.

Rajendran, S., Wanale, S.G., Gacem, A., Yadav, V.K., Ahmed, I.A., Algethami, J.S., Kakodiya, S.D., Modi, T., Alsuhaibani, A.M., Yadav, K.K., Cavalu, S., 2023. Nanostructured iron oxides: structural, optical, magnetic, and adsorption characteristics for cleaning industrial effluents. Crystals 13, 472. https://doi.org/10.3390/cryst13030472.

Schreck, E., Viers, J., Blondet, I., Auda, Y., Macouin, M., Zouiten, C., Freydier, R., Duffechou, G., Chmeleff, J., Darrozes, J., 2020. Tillandsia usneoides as biomonitors of trace elements contents in the atmosphere of the mining district of Cartagena-La Union ′ (Spain): new insights for element transfer and pollution source tracing. Chemosphere 241, 124955. https://doi.org/10.1016/j.chemosphere.2019.124955.

Singh, A., Sanjeeb, K.S., 2014. Magnetic nanoparticles: a novel platform for cancer theranostics. Drug Discov. Today 19, 474–481.

Singh, R.P., Handa, R., Manchanda, G., 2021. Nanoparticles in sustainable agriculture: an emerging opportunity. J. Contr. Release 329, 1234–1248.

Sun, X., Li, P., Zheng, G., 2021. Cellular and subcellular distribution and factors influencing the accumulation of atmospheric Hg in *Tillandsia usneoides* leaves. J. Hazard Mater. 414, 125529 https://doi.org/10.1016/j.jhazmat.2021.125529.

Tombuloglu, H., Slimani, Y., Tombuloglu, G., Almessiere, M., Baykal, A., 2019. Uptake and translocation of magnetite (Fe3O4) nanoparticles and its impact on photosynthetic genes in barley (*Hordeum vulgare* L.). Chemosphere 226, 110–122.

Ursache-Oprisan, M., Focanici, E., Creanga, D., Caltun, O., 2011. Sunflower chlorophyll levels after magnetic nanoparticle supply. Afr. J. Biotechnol. 10 (36), 7092–7098. https://doi.org/10.5897/AJB11.477.

Verma, P.C., Alemani, M., Gialanella, S., Lutterotti, L., Olofsson, U., Straffelini, G., 2016. Wear debris from brake system materials: a multi-analytical characterization approach. Tribol. Int. 97, 249–259.

Vose, P.B., 1982. Iron nutrition in plants: a world overview. J. Plant Nutr. 5, 233–249. https://doi.org/10.1080/01904168209362954.

Wang, H.H., Kou, X.M., Pei, Z.G., et al., 2011. Physiological effects of magnetite (Fe3O4) nanoparticles on perennial ryegrass (Lolium perenne L.) and pumpkin (Cucurbita mixta) plants. Nanotoxicology 5, 30–42.

Wohlfart, S., Gelperina, S., Kreuter, J., 2012. Transport of drugs across the blood–brain barrier by nanoparticles. J. Control. Release. 161, 264–273.

Yadav, V.K., Ali, D., Khan, S.H., Gnanamoorthy, G., Choudhary, N., Yadav, K.K., Thai, V. N., Hussain, S.A., Manhrdas, S., 2020. Synthesis and characterization of amorphous iron oxide nanoparticles by the sonochemical method and their application for the remediation of heavy metals from wastewater. Nanomaterials 10, 1551. https://doi.org/10.3390/nano10081551.

Yan, L., Li, P., Zhao, X., Ji, R., Zhao, L., 2020. Physiological and metabolic responses of maize (Zea mays) plants to Fe3O4 nanoparticles. Sci. Total Environ. 718, 137400 https://doi.org/10.1016/j.scitotenv.2020.137400. ISSN 0048-9697.

Zhang, Q., Lu, D., Wang, D., Yang, X., Zuo, P., Yang, H., Fu, Q., Liu, Q., Jiang, G., 2020. Separation and tracing of anthropogenic magnetite nanoparticles in the urban atmosphere. Environ. Sci. Technol. 54 (15), 9274–9284.

Zhu, Y., Wu, J., Chen, M., Liu, X., Xiong, Y., Wang, Y., Feng, T., Kang, S., Wang, X., 2019. Recent advances in the biotoxicity of metal oxide nanoparticles: impacts on plants, animals and microorganisms. Chemosphere 237, 124403. https://doi.org/10.1016/j.chemosphere.2019.124403.